

INTERACTION OF LASER RADIATION WITH MATTER

PACS numbers: 72.15.–v; 42.65.Re; 42.62.Cf
DOI: 10.1070/QE2015v045n10ABEH015729

Limits of applicability of a two-temperature model under nonuniform heating of metal by an ultrashort laser pulse

D.S. Polyakov, E.B. Yakovlev

Abstract. **The heating of metals (silver and aluminium) by ultrashort laser pulses is analysed proceeding from a spatially nonuniform kinetic equation for the electron distribution function. The electron subsystem thermalisation is estimated in a wide range of absorbed pulse energy density. The limits of applicability are determined for the two-temperature model.**

Keywords: *femtosecond pulse, thermalisation time, two-temperature model.*

1. Introduction

It is well known that irradiation of metal targets by a high-power laser pulse results in a strong overheating of the electron subsystem relative to the lattice one. Descriptions of this metal state usually rely on a so-called two-temperature model (TTM), which contains a system of coupled heat conduction equations for electrons and the lattice [1]. Strictly speaking, the electron subsystem may be described using the notion of temperature only under local quasi-equilibrium conditions. When a metal is irradiated by an ultrashort laser pulse (USP), this situation takes place after some time (the thermalisation time), which depends on the kind of metal and its processing method. The presently available experimental [2–4] and theoretical [5, 6] works give estimates of the thermalisation time under pulsed irradiation with an absorbed energy density $Q_a \ll 2$ mJ cm^{-2} when the thermalisation proceeds primarily after the cessation of irradiation and may last for hundreds of femtoseconds (up to picoseconds). We note that the experiment of Ref. [2] studied a metallic gold film, the authors of Ref. [3] dealt with a bulk metal (bismuth) and paper [4] was concerned with silver nanoparticles on a graphite substrate. According to Ref. [6], the electron-to-lattice energy transfer rate may be lower under these conditions, which is levelled out with increasing intensity of excitation laser pulses.

From the technological viewpoint, the range $Q_a > 2$ mJ cm^{-2} is of greater interest. The applications of USPs involving metal ablation [7] (for $Q_a > 100$ mJ cm^{-2}) are commonly known. Recently interest was aroused under nondestructive irradiation of metals by femtosecond pulses (approximately in the range 2 mJ cm^{-2} $< Q_a <$ 20 mJ cm^{-2}). For instance, the possibility of producing chemical etching-resistant domains by irradiation of a chromium film by single USPs was recently demonstrated in Ref. [8]. According to the hypothesis expressed in Ref. [9], the appearance of resistance to chemical etching may be due to the formation of a protective oxide layer, whose growth is essentially related to the thermal electron emission, and therefore the investigation of the correctness of TTM applicability is highly important in this case.

The authors of theoretical papers, Refs [5, 6], which lean upon the kinetic equation, restrict themselves to the treatment of spatially uniform problems. Accordingly, the critical issues of energy transport in USP-irradiated metals were investigated only in the framework of the TTM, whose exact limits of applicability have not been determined in this respect. Also little studied is the evolution of the distribution function during the course of the pulse for $Q_a > 2$ mJ cm^{-2}, when its variation is caused by the competition between excitation (absorption of radiation photons) and relaxation (electron–electron collisions), whereas the magnitude of the electron emission current is determined by precisely the form of the distribution function.

The objective of our work is to analyse the heating of bulk metals by USPs proceeding from the spatially nonuniform Boltzmann kinetic equation for the electron distribution function and to determine the limits of TTM applicability.

2. Formulation of the problem

Basic model equations. We consider one-band metals with a parabolic dispersion law. A good example of a one-band metal is provided by aluminium, in which the energy gap between the conduction and valence bands is equal to about 60 eV. For noble metals, this model is most suitable for silver, in which the d-band top is spaced at an energy of 3.8 eV from the Fermi level [10].

The approach to the description of USP-driven metal heating considered in the present work consists in the replacement of the heat conduction equation with the kinetic equation for the distribution function. The model is supplemented with an equation which describes the radiation intensity distribution inside the metal. Also included is the emergence of a longitudinal electric field owing to the nonuniformity of the electron distribution. Therefore, the system of equations to be solved, in combination with the initial and boundary conditions, is of the form

$$\frac{\partial f}{\partial t} + v_x \frac{\partial f}{\partial x} + eE_x \frac{\partial f}{\partial p_x} = \left(\frac{\partial f}{\partial t}\right)_{\text{abs}} + \left(\frac{\partial f}{\partial t}\right)_{\text{e-e}} + \left(\frac{\partial f}{\partial t}\right)_{\text{e-ph}}, \quad (1)$$

$$c_{\text{i}} \frac{\partial T_{\text{i}}}{\partial t} = \left(\frac{\partial E_{\text{i}}}{\partial t}\right)_{\text{e-ph}}, \quad (2)$$

D.S. Polyakov, E.B. Yakovlev ITMO University, Kronverkskii prosp. 49, 197101 St. Petersburg, Russia; e-mail: polyakovdmitry1988@gmail.com, yak@lastech.ifmo.ru

Received 12 December 2014; revision received 7 July 2015
Kvantovaya Elektronika **45** (10) 917–926 (2015)
Translated by E.N. Ragozin

$$\frac{\partial E_x(x,t)}{\partial x} = -\frac{e}{\varepsilon\varepsilon_0}\int (f_0 - f)\frac{2\mathrm{d}\boldsymbol{p}}{(2\pi\hbar)^3}, \tag{3}$$

$$-\frac{1}{\hbar\omega}\frac{\partial q(x,t)}{\partial x} = \int\left(\frac{\partial f}{\partial t}\right)_+ \frac{2\mathrm{d}\boldsymbol{p}}{(2\pi\hbar)^3}, \tag{4}$$

$$f(x,\boldsymbol{p},0) = f_0 = \left[\exp\left(\frac{E(\boldsymbol{p}) - \mu(T_0)}{k_\mathrm{B}T_0}\right) + 1\right]^{-1},$$

$$p_x f(0,\boldsymbol{p},t) = \int_{p_x^* < 0} (1 - K(\boldsymbol{p}^*))p_x^* f(0,\boldsymbol{p}^*,t)R(\boldsymbol{p}^*,\boldsymbol{p})\,\mathrm{d}\boldsymbol{p}^*,$$

$$T_\mathrm{i}(0,t) = T_0,\ \left.\frac{\partial T_\mathrm{i}}{\partial x}\right|_{x=0} = 0,\ E_x(\infty,t) = 0,\ q(0,t) = q_0(t),$$

where $f = f(x,\boldsymbol{p},t)$ is the electron distribution function such that $\mathrm{d}N_\mathrm{e} = 2f\mathrm{d}\boldsymbol{p}\mathrm{d}\boldsymbol{r}/(2\pi\hbar)^3$ is the number of electrons in an element in the six-dimensional phase space $(\boldsymbol{r},\boldsymbol{p})$ of coordinates and momenta; the x axis is directed normally to the surface into the metal bulk (we consider the one-dimensional case); t is the time; v_x is the projection of the electron velocity onto the x axis; E_x is the projection of electric intensity onto the x axis; e is the electron charge; the terms $(\partial f/\partial t)_\mathrm{abs}$, $(\partial f/\partial t)_\mathrm{e-e}$ and $(\partial f/\partial t)_\mathrm{e-ph}$ describe the radiation absorption, electron–electron and electron–phonon collisions, respectively; $T_\mathrm{i} = T_\mathrm{i}(x,t)$ is the lattice temperature; $(\partial E_\mathrm{i}/\partial t)_\mathrm{e-ph}$ is the variation of volume energy density of the lattice due to the interaction with electrons; c_i is the heat capacity of a unit volume of the lattice; ε_0 is the dielectric constant; ε is the permittivity; $q(x,t)$ is the radiation power density; $\hbar$ is the reduced Planck constant; ω is the incident radiation frequency; the expression in the right side of Eqn (4) defines the number of photons absorbed per unit time in a unit volume (for more details, see below); q_0 is the power density at the metal surface; $E(\boldsymbol{p})$ is the electron energy; μ is the chemical potential; k_B is the Boltzmann constant; T_0 is the initial temperature; the function $K(\boldsymbol{p})$ is the probability that an electron with a momentum $\boldsymbol{p}$ escapes from the metal in the collision with the surface; and the function $R(\boldsymbol{p},\boldsymbol{p}^*)$ is the probability that the $\boldsymbol{p}^*$ electron is scattered by the surface into the $\boldsymbol{p}$ state.

Equation (1) is of the form of a standard kinetic equation, whose right-hand side includes collisions of three types: absorption of radiation photons, electron–electron and electron–phonon collisions. The phonon subsystem is assumed to be in the state of equilibrium, and therefore the ordinary heat conduction equation (2) is employed to describe its heating. The expression for the term which describes the electron–lattice energy transfer for an arbitrary electron distribution function is given in Ref. [11]. Equation (3) was earlier employed to estimate the magnitude of the electric field [12]. The boundary condition for the kinetic equation accounts for the possibility of electron emission. In the simplest case it is assumed that all electrons that reach the surface and have sufficient energy escape from the metal.

Radiation absorption. The variation of the distribution function occurring under the absorption of radiation photons (with the inclusion of multiphoton processes) is described by the expression

$$\left(\frac{\partial f}{\partial t}\right)_\mathrm{abs} = \sum_n \int [w_n(\boldsymbol{p}_{+n},\boldsymbol{p})f_{+n}(1-f) - w_n(\boldsymbol{p},\boldsymbol{p}_{+n})f(1-f_{+n})]\frac{2\mathrm{d}\boldsymbol{p}_{+n}}{(2\pi\hbar)^3},$$

where $f_{+n} = f(x,\boldsymbol{p}_{+n},t)$; $\boldsymbol{p}_{+n}$ is the electron momentum after (or prior to) the absorption of n photons; and $w_n(\boldsymbol{p},\boldsymbol{p}_{+n})$ are the probabilities per unit time that a $\boldsymbol{p}$ electron undergoes n-photon absorption with the transition to the $\boldsymbol{p}_{+n}$ state.

The probabilities $w_n(\boldsymbol{p},\boldsymbol{p}_{+n})$ are taken in the form

$$w_n(\boldsymbol{p},\boldsymbol{p}_{+n}) = \sigma_n\left(\frac{q}{\hbar\omega}\right)^n \frac{\pi^2\hbar^3}{m_\mathrm{e}}\frac{\delta(E(\boldsymbol{p}_{+n}) - E(\boldsymbol{p}) - n\hbar\omega)}{|\boldsymbol{p}_{+n}|},$$

where σ_n are the multiphoton absorption cross sections [13]; m_e is the effective electron mass; and $\delta(E(\boldsymbol{p}_{+n}) - E(\boldsymbol{p}) - n\hbar\omega)$ is the delta function which ensures energy conservation.

The integrand in the right-hand side of Eqn (4) is defined by the formula

$$\left(\frac{\partial f}{\partial t}\right)_+ = \sum_n n\int w_n(\boldsymbol{p},\boldsymbol{p}_{+n})f(1-f_{+n})\frac{2\mathrm{d}\boldsymbol{p}_{+n}}{(2\pi\hbar)^3}.$$

By using the estimates of σ_n from Ref. [13] it may be shown that the multiphoton processes should be taken into account for $q > 10^{12}$ W cm^{-2}. In the case of one-photon absorption, the approach described here yields an exponential absorption with a penetration depth $\delta = (\sigma_1 n_1^*)^{-1}$, where n_1^* is the density of electrons in the energy range from $E_\mathrm{F} - \hbar\omega$ to E_F (E_F is the Fermi energy).

Electron–electron collisions. The electron–electron collision integral may be presented in the following form [14]:

$$\left(\frac{\partial f}{\partial t}\right)_\mathrm{e-e} = \int [f'f_1'(1-f)(1-f_1) - ff_1(1-f')(1-f_1')] \times \frac{|\boldsymbol{p}_1 - \boldsymbol{p}|}{m_\mathrm{e}}\sigma_\Omega \mathrm{d}\Omega\frac{2\mathrm{d}\boldsymbol{p}_1}{(2\pi\hbar)^3},$$

where $f_1 = f_1(x,\boldsymbol{p}_1,t)$; $f' = f'(x,\boldsymbol{p}',t)$; $f_1' = f_1'(x,\boldsymbol{p}_1',t)$; σ_Ω is the differential scattering cross section; and $\mathrm{d}\Omega$ is an element of the solid angle.

The electron–electron interaction is described by the screened Coulomb potential with the shielding radius taken from the Thomas–Fermi model [15]. The cross section σ_Ω for the indicated type of potential is calculated in the first Born approximation (see, for instance, Ref. [16]).

Electron–phonon collisions. The electron–phonon collision integral which takes into account the emission and absorption of acoustic phonons is defined by the relation [17]:

$$\left(\frac{\partial f}{\partial t}\right)_\mathrm{e-ph} = \int w_\mathrm{e-ph}(\boldsymbol{q})\{[f_{+q}(1-f)(N(\boldsymbol{q})+1) - f(1-f_{+q})N(\boldsymbol{q})] \times \delta(E(\boldsymbol{p}+\boldsymbol{q}) - E(\boldsymbol{p}) - \hbar\Omega(\boldsymbol{q})) + [f_{-q}(1-f)N(\boldsymbol{q}) - f(1-f_{-q})(N(\boldsymbol{q})+1)]\delta(E(\boldsymbol{p}-\boldsymbol{q}) - E(\boldsymbol{p}) + \hbar\Omega(\boldsymbol{q}))\}\frac{\mathrm{d}\boldsymbol{q}}{(2\pi\hbar)^3},$$

where $f_{+q} = f(x,\boldsymbol{p}+\boldsymbol{q},t)$; $f_{-q} = f(x,\boldsymbol{p}-\boldsymbol{q},t)$; $N(\boldsymbol{q})$ is the phonon distribution function; $\boldsymbol{q}$ is the phonon quasi-momentum; and $w_\mathrm{e-ph}(\boldsymbol{q}) \propto |\boldsymbol{q}|$ defines the absorption (emission) probabilities of acoustic phonons [17], whose dispersion law is taken in the Debye approximation.

The results of the numerical solution of the system of equations (1)–(4) for different processing modes are compared with the TTM-based calculations reliant on traditional formulation of the problem (see, for instance, Ref. [18]):

$$c_e(T_e)\frac{\partial T_e}{\partial t} - \frac{\partial}{\partial x}\left(k_e(T_e, T_i)\frac{\partial T_e}{\partial t}\right) = q_v - G(T_e - T_i),$$

$$c_i\frac{\partial T_i}{\partial t} = G(T_e - T_i),$$

$$k_e\frac{\partial T_e}{\partial x}\bigg|_{x=0} = 0,$$

$$T_e(\infty, t) = T_0,$$

$$T_e(x, 0) = T_i(x, 0) = T_0,$$

where c_e is the lattice specific heat; k_e is the electron thermal conductivity coefficient; q_v is the thermal source for electrons due to radiation absorption; and G is the electron lattice heat exchange coefficient. In these calculations, account was taken of the dependence of TTM parameters on the electron and lattice (in the case of electron heat conductivity) temperatures presented in the next Section.

The thermophysical metal characteristics (the electron heat capacity, the electron heat conductivity, and the electron–lattice heat exchange coefficient) are calculated proceeding from the same microscopic parameters that were employed in the solution of the system of equations (1)–(4) (we imply, for instance, the electron–electron interaction screening radius, the probabilities of electron–phonon collisions, the approximation of band electron spectrum, etc.). Therefore, by comparing the data of TTM calculations with the data of simulations in the framework of the model based on the kinetic equation, it is possible to estimate the error of the data of TTM calculations and thereby determine the limits of its applicability.

3. Main results and their discussion

We have performed simulations for two metals: silver and aluminium. In both cases, the effective electron mass was assumed to be equal to the electron mass in vacuum. The characteristic radiation penetration depth in the exponential absorption was also assumed to be the same for both metals and equal to $\delta = 10$ nm. Therefore, in the framework of model assumptions the individual distinguishing characteristics of the metals are primarily due to the density n_e of conduction electrons, which is equal to 5.86×10^{22} cm^{-3} for silver and 18×10^{22} cm^{-3} for aluminium. The temporal dependence of absorbed radiation power density (the pulse shape) was of the form

$$q_0(t) = \frac{Q_a}{t_0^2}t\exp\left(-\frac{t}{t_0}\right),$$

where $t > 0$ and t_0 is a parameter with the meaning of pulse rise time [the total pulse duration is $t_p = 4t_0$ if the instant of pulse cessation is taken at a level of 20% of the peak value of the $q_0(t)$ dependence].

Our calculations were carried out for the radiation with a wavelength of 1.06 μm (the corresponding photon energy is $\hbar\omega = 1.2$ eV).

Numerical simulation technique. The use of finite-difference numerical simulation techniques is seriously hindered due to the complex structure of multidimensional collision integrals and a large number of arguments of the distribution function. In this situation there is good reason to resort to so-called direct statistical simulation methods.

The simulated medium is represented by a large set of particles, whose initial coordinates and momenta are defined in accordance with the initial form of their distribution function. Next, the temporal evolution of the system is determined using some statistical procedure to simulate the physical processes that are responsible for variations of particle coordinates and momenta (collisions and collisionless motion). To calculate electron–electron collisions, use is made of the computational scheme described in Ref. [19] (a particle-in-cell technique), which is supplemented by the condition that electron transitions to occupied states are forbidden. Electron–phonon collisions and photon absorption are modelled proceeding from the corresponding event probabilities, which may be explicitly obtained for each electron. At every time step, collisionless motion is modelled by calculating the variations of electron's coordinates in accordance with its velocity.

The direct statistical simulation technique is used in the solution of Eqn (1) and in the calculation of the integrals that appear in the right-hand sides of Eqns (2)–(4). The subsequent solution of Eqns (2)–(4) is performed using finite-difference methods.

We emphasise that the electron–electron collision simulation scheme employed in our work opens the door to the calculation of electron–electron collision frequencies for equilibrium conditions in a broad temperature range required in the calculation of the electron thermal conductivity coefficient.

Equilibrium electron–electron collision frequencies. We give the data on electron–electron collision frequencies under equilibrium conditions as a confirmation of the adequacy of the numerical simulation technique employed in our work. According to Refs [20, 21], in the low-temperature domain the frequencies of collisions between electrons with a momentum $\boldsymbol{p}$ and other electrons, which determine the electron thermal conductivity, the following analytical dependence holds good:

$$\nu_{e-e}(p, T_e) = \frac{e^4}{16\pi^3\hbar^4\varepsilon_0^2}\frac{k^2}{v^3 q_s^2}\left(\frac{2k}{4k^2 + q_s^2} + \frac{1}{q_s}\arctan\left(\frac{2k}{q_s}\right)\right)$$

$$\times\left[\pi^2 + \left(\frac{E - E_F}{k_B T_e}\right)^2\right](k_B T_e)^2, \qquad (5)$$

where $p = |\boldsymbol{p}|$; $k = p/\hbar$, $v = p/m_e$ are the moduli of the electron momentum, wave vector and velocity; and $q_s = 1/r_s$ is the reciprocal of the Thomas–Fermi screening radius.

Figure 1 shows the calculated dependence $\nu_{e-e}(p_F, T_e)$ (p_F is the Fermi momentum), which is compared with the analytical dependence (5) for silver and aluminium. As is clear from Fig. 1, the analytical dependence and our simulations agree nicely in the temperature range $T_e < 0.1T_F$ (T_F is the Fermi temperature equal to 6.4×10^4 K for aluminium and to 13.5×10^4 K for silver). For $T_e > 0.1T_F$, as would be expected, the parabolic dependence saturates and the collision frequency increases slower than the parabola. For aluminium, the frequencies are approximately 2.5 times lower than for silver, which is primarily because the screening radius for electron–electron interactions is shorter.

Thermophysical metal parameters used in TTM calculations. As already noted, the thermophysical metal parameters which appear in the system of TTM equations must be correctly defined for reaching the objectives of our work. Figure 2

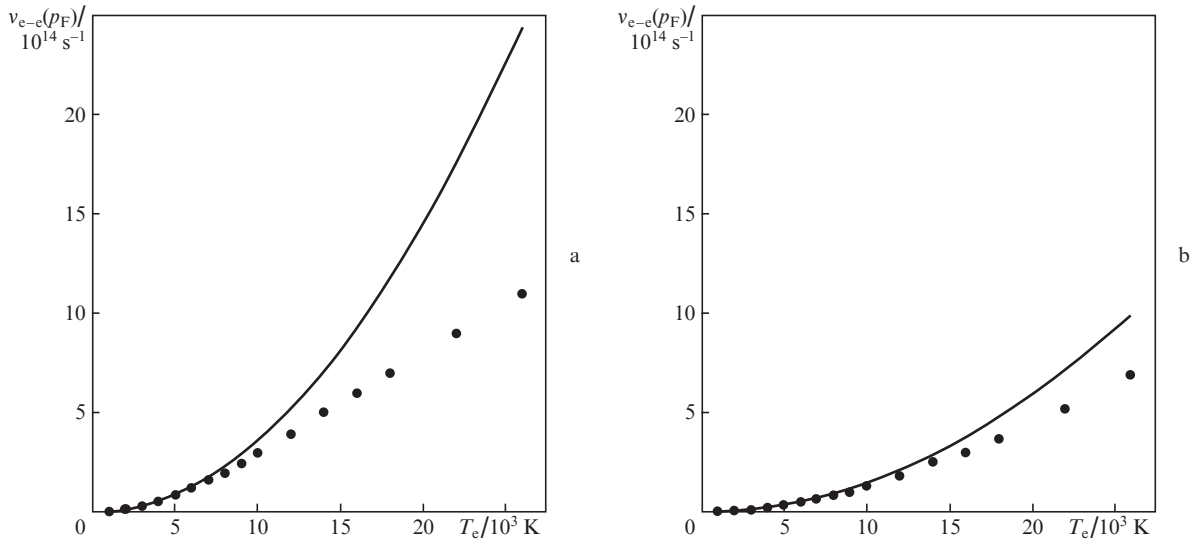

Figure 1. Temperature dependences of electron–electron collision frequencies [points stand for simulations and solid lines for analytical dependence (5)] for (a) silver and (b) aluminium.

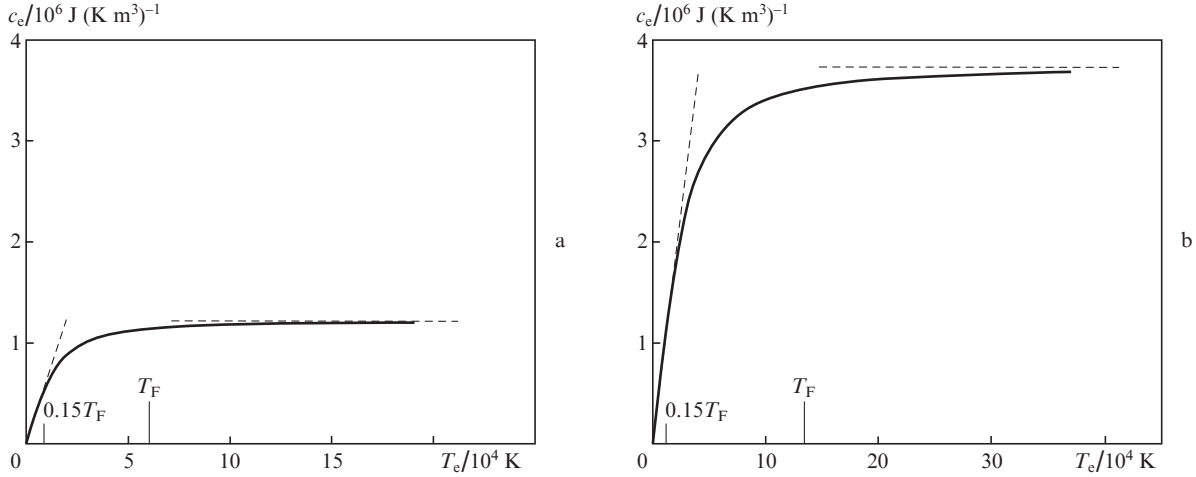

Figure 2. Temperature dependences of the heat capacity of the electron gas for (a) silver and (b) aluminium.

shows the temperature dependences of electron heat capacity for silver and aluminium in a broad electron temperature range. In accordance with the previously made assumptions, our calculations were performed in the framework of a one-band model with a parabolic dispersion law. One can see from Fig. 2 that the linear dependence of the electron heat capacity on the electron temperature holds for $T_e < 0.15T_F$. For high ($T_e > T_F$) temperatures, the heat capacity approaches a constant value $c_e = {}^3/_2 n_e k_B$, which corresponds to the value of the heat capacity of a classical ideal gas. Figure 3 shows the calculated temperature dependences of the electron thermal conductivity coefficient k_e due to electron–electron and electron–phonon collisions. Figure 3a shows the $k_e(T_e)$ dependence for silver for different lattice temperatures. Figure 3b shows the calculated $k_e(T_e)$ dependence for aluminium at room temperature of the lattice and a comparison with the data of Ref. [11]. With reference to Fig. 3, the agreement between the calculations may be regarded as satisfactory.

A well pronounced feature is observed in the case of silver: a clearly nonmonotonic behaviour of the $k_e(T_e)$ dependence (like in Ref. [11] for gold). This behaviour is easily understood when the temperature dependence of the thermal conductivity is approximated by the Drude formula

$$k_e = \frac{c_e \langle v^2 \rangle}{3(\nu_{e-ph}^{eff} + \nu_{e-e}^{eff})},$$

where $\langle v^2 \rangle$ is the average square of the electron velocity; and ν_{e-ph}^{eff} and ν_{e-e}^{eff} are the effective electron–phonon and electron–electron collision frequencies. Prevalent at low temperatures is the electron–phonon scattering ($\nu_{e-ph}^{eff} \gg \nu_{e-e}^{eff}$), whose intensity is independent of the electron temperature. Since $c_e \propto T_e$ and $\langle v^2 \rangle$ depends only slightly on T_e in the low-temperature domain, the initial growth of the thermal conductivity obeys a linear law. As the temperature increases, the electron– electron scattering becomes significant ($\nu_{e-e}^{eff} \propto T_e^2$), which tends to decrease the thermal conductivity. This accounts for the saturation of the linear dependence, the appearance of a maximum of the thermal conductivity, and its subsequent decrease. On a further increase in the electron temperature, the growth of ν_{e-e}^{eff} is slower than the parabolic

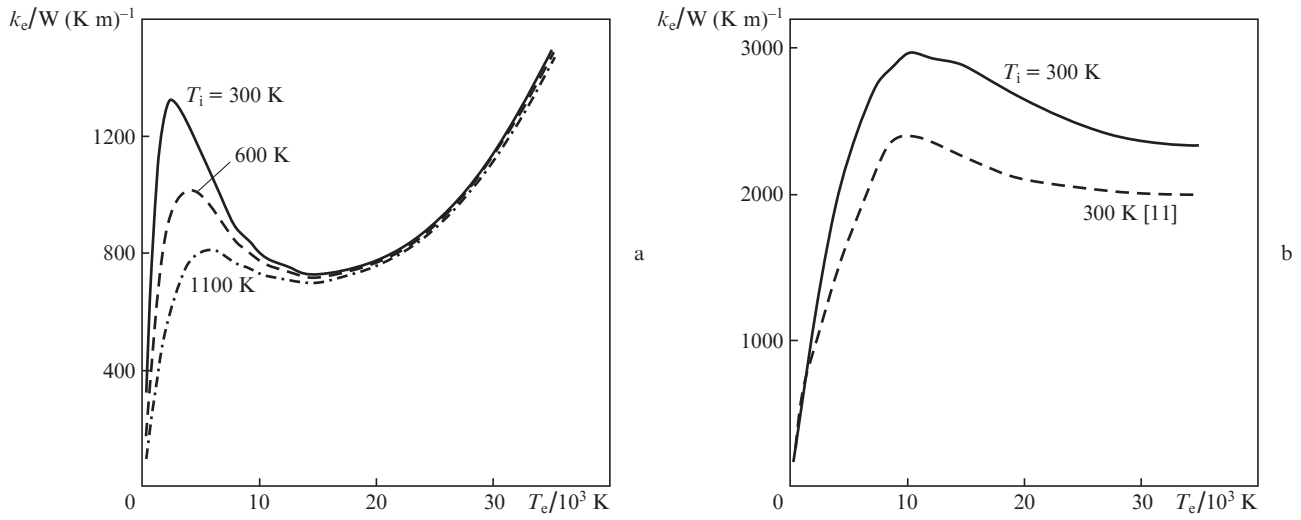

Figure 3. Dependences of the electron thermal conductivity on the electron temperature for different lattice temperatures for (a) silver and (b) aluminium.

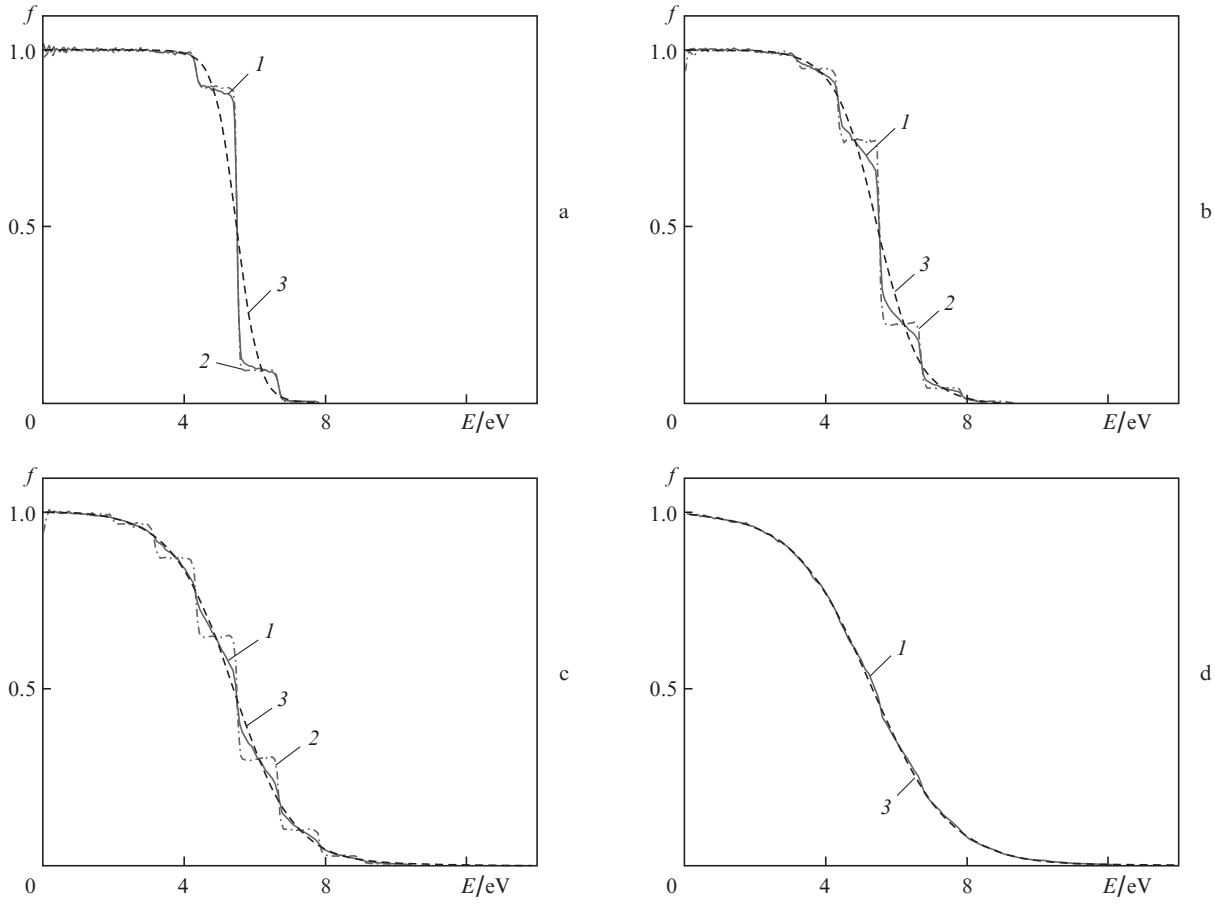

Figure 4. Electron energy distribution function in silver irradiated by a pulse with the parameters Q_a = 30 mJ cm^{-2}, t_0 = 40 fs at the surface, which was calculated with the inclusion of excitation and relaxation (*1*) and without relaxation (*2*), as well as the equilibrium distribution function (*3*) at the points in time (a) 7, (b) 14, (c) 21 and (d) 28 fs.

one (see Fig. 1), while the growth of $\langle v^2 \rangle$ becomes appreciable and c_e continues to grow. Consequently, beginning from some point, the $k_e(T_e)$ dependence attains a local minimum (for $T_e \approx$ 15 kK for silver) and begins to grow monotonically. A similar feature also takes place for aluminium, but it is less pronounced.

The dependence on the ion temperature manifests itself only in the low-temperature domain, where electron–phonon scattering is significant. In this domain $k_e(T_e, T_i) \propto T_i^{-1}$, because $\nu_{e-ph}^{eff} \propto T_i$. The dependence of electron thermal conductivity on the ion temperature is insignificant in the electron-temperature domain where the electron–electron scattering prevails.

In the case of a one-band electron spectrum, the G coefficient is hardly dependent on the electron and lattice temperatures. The G values for silver and aluminium were found to be equal to 3.5×10^{16} W (K m^3)$^{-1}$ and 3×10^{17} W (K m^3)$^{-1}$, respectively.

Estimates of thermalisation time. From the computational standpoint, the solution of problem (1)–(4) in its complete formulation is a laborious task, which requires considerable computational time. It is expedient to preliminarily estimate the thermalisation time in a broad range of a pulse energy density. These estimates can be obtained by neglecting the energy transport and electron–phonon collisions (in view of the smallness of energy transfer in a single collision) in Eqn (1), i.e. by considering only the excitation (the absorption of radiation photons) and the relaxation due to electron–electron collisions.

At first we briefly describe the mechanism of the distribution function variation. Figure 4 shows the typical evolution of the electron energy distribution function in silver near the surface under irradiation by a pulse with $Q_a = 30$ mJ cm^{-2} and $t_0 = 40$ fs. At the initial stage of irradiation, the excitation gives rise to steps of width equal to the photon energy ($\hbar\omega = 1.2$ eV). Subsequently, electron–electron collisions result in a gradual step smearing, and some time later the distribution function becomes close to the equilibrium one. A similar mechanism was also described in Refs [5, 6]; it corresponds to experimental ultrafast emission spectroscopy data obtained in Refs [2, 4] at a low excitation pulse energy density. In Fig. 5, the calculated distribution function (in this case, electron–phonon collisions and the energy transfer are included in the simulation for a more correct comparison) is compared with the distribution function obtained in the experiment of Ref. [2] for gold for $Q_a \approx 0.3$ mJ cm^{-2}, $t_p = 180$ fs, and $\hbar\omega = 1.84$ eV. One can see that the agreement is quite satisfactory. For a measure of the departure of the distribution function from the equilibrium one, we introduce the quantity

$$\mathrm{Cr}(t) = \frac{\int_0^\infty |f - f_0|\, g(E)\,\mathrm{d}E}{\int_0^\infty f_0 g(E)\,\mathrm{d}E},$$

where f is the current distribution function; f_0 is the equilibrium distribution function which corresponds to the same internal energy; and $g(E)$ is the level density. In accordance with its definition, $\mathrm{Cr}(t)$ is the ratio between the area confined between the curves corresponding to the equilibrium and non-equilibrium distribution functions and the total area under the distribution function [i.e. the electron density on the strength of the normalisation condition of the function $g(E)$]. The $\mathrm{Cr}(t)$ function increases to some maximal value with a subsequent decay. The thermalisation time τ_0 is estimated using the following criterion: $\mathrm{Cr}(\tau_0) = 0.2\,\mathrm{Cr}_{max}$ [Cr_{max} is the maximal value of $\mathrm{Cr}(t)$].

Figure 6a shows the dependence of τ_0 on the absorbed energy density near the metal surface. For $Q_a = 100$ mJ cm^{-2} (the characteristic value of metal ablation threshold) the thermalisation time at the surface is equal to 17 fs for silver and to 30 fs for aluminium. With an increase in energy density, the relaxation time shortens slowly to flatten out at 13 and 23 fs for silver and aluminium, respectively. As the energy density decreases, the thermalisation time increases. Since the energy density decreases with depth, the thermalisation time in the metal interior will be longer than at the surface. Figure 6b shows the variation of the time τ_0 with depth for $Q_a = 100$ mJ cm^{-2}.

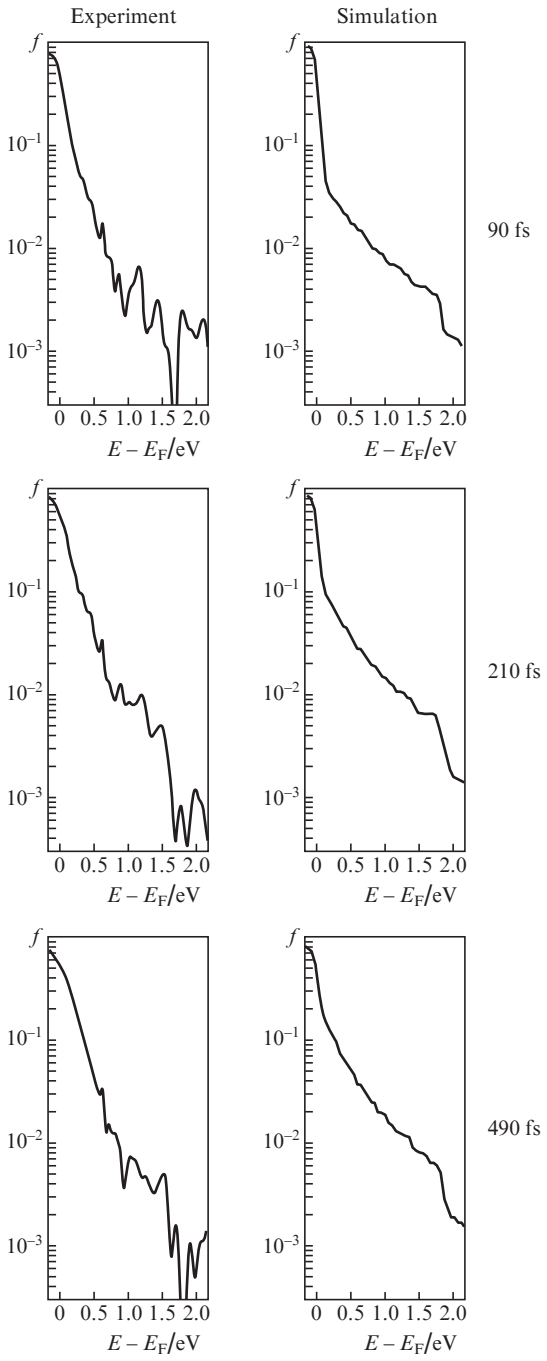

Figure 5. Comparison of the calculated electron energy distribution function with the distribution obtained in the experiment of Ref. [2] for gold at different points in time.

One can see that the thermalisation time changes only little over the skin layer depth ($\delta = 10$ nm) both for silver and aluminium. In deeper layers the relaxation lengthens out to tens–hundreds of femtoseconds, but the heating of these layers is relatively small.

The emission current density is directly determined by the form of the distribution function near the metal surface. In this case, it is clear that the behaviour of the distribution function in the domain $E > U_0$ (U_0 is the potential barrier at the metal boundary) is the decisive factor. The relaxation times given above were obtained proceeding from the criterion that took into account the departures of the distribution function

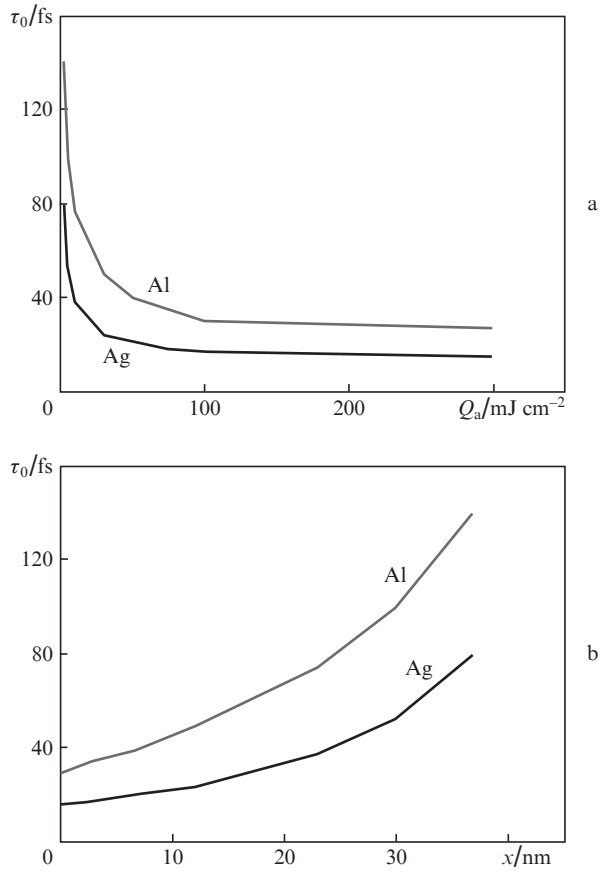

Figure 6. Dependence of the near-surface relaxation time on the absorbed energy density for $t_0 = 40$ fs (a) and on the depth for $Q_a = 100$ mJ cm^{-2} and $t_0 = 40$ fs (b) for silver and aluminium.

from the equilibrium one over the entire energy range. In view of this, there is good reason to estimate the effect of the nonequilibrium state of the electron distribution on the emission current density with the use of another criterion, specifically, by investigating the relative error of calculating the emission current from the equilibrium distribution:

$$\mathrm{Cr}_{\mathrm{em}}(t) = \frac{|j_e(f) - j_e(f_0)|}{j_e(f)},$$

where

$$j_e(f) = \frac{4\pi e m_e}{(2\pi\hbar)^3}\int_{U_0}^{\infty}(E - U_0) f_s(E)\,\mathrm{d}E \qquad (6)$$

is the emission current density and $f_s(E)$ is the distribution function at the surface. When $f_s = f_0$ and the inequality $U_0 - \mu(T_e) \gg k_B T_e$ is obeyed, formula (6) passes into the Richardson thermionic emission law:

$$j_R = BT_e^2 \exp\left(-\frac{A_0}{k_B T_e}\right),$$

where $B = 4\pi e m_e k_B^2/(2\pi\hbar)^3 = 120$ A (cm K)$^{-2}$, and $A_0 = U_0 - E_F$ is the work function.

The 'emission' relaxation time τ_0^{em} is defined by the following criterion: $\mathrm{Cr}_{\mathrm{em}}(\tau_0^{\mathrm{em}}) = 0.15$. Figure 7 shows the dependence of τ_0^{em} on the absorbed energy density. One can see that the 'emission' relaxation time is shorter than the relaxation time τ_0. The difference is most conspicuous in the low energy

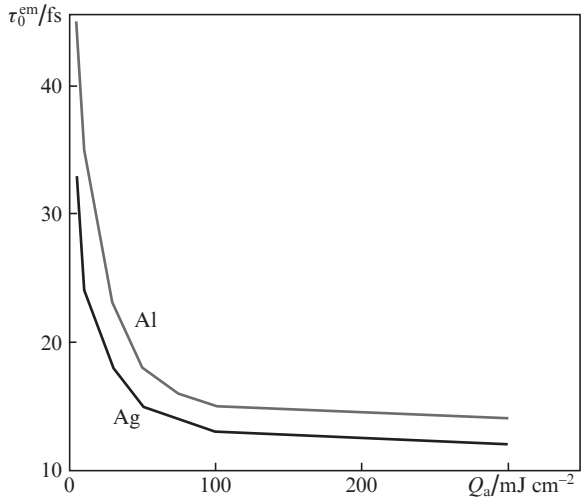

Figure 7. 'Emission' relaxation time at the surface as a function of absorbed energy density for $t_0 = 40$ fs for silver and aluminium.

density domain. This difference is due to the fact that the electron–electron collision frequencies are higher for high-energy electrons, and the 'tail' of the distribution function therefore forms faster. It is clear that the main contribution to the total number of emitted electrons is made by the instants of time when the electron temperature is close to the maximal temperature. The maximal temperature is attained close to the end of a pulse, i.e. when $t \approx t_p$. Since $\tau_0^{\mathrm{em}} \ll t_p$ ($t_p = 160$ fs), the contribution of nonequilibrium electrons to the total number of electrons emitted from the surface may be neglected.

Therefore, preceding from our estimates it is possible to draw a conclusion that the electron thermalisation occurs rather rapidly at an energy input close to the ablation threshold (see Fig. 6) and that the effect of the nonequilibrium state of the electron distribution on metal heating is small. The range of lower energy densities invites further investigation. As regards emission effects, it is valid to note that the electron emission may be described throughout the energy density range (2–300 mJ cm^{-2}) under discussion using the notion of temperature that corresponds to the volume electron energy density at the metal surface. We emphasise that the very value of this temperature with the inclusion of energy transport may differ from TTM predictions.

Dynamics of electron and lattice temperatures. The inclusion of energy transport has no significant effect on the above estimates of thermalisation time. Figure 8a shows the time dependences of the electron temperature at the silver surface calculated proceeding from the TTM [$T_e^{\mathrm{ttm}}(t)$] and the kinetic equation [$T_e^{\mathrm{kin}}(t)$] during the course of a pulse with the parameters $Q_a = 5$ mJ cm^{-2}, $t_0 = 40$ fs. In the domain $t < t_0$ (i.e. when the distribution is nonequilibrium), by the temperature is meant the quantity related to the internal energy by the same equation as in the case of equilibrium distribution. Figure 8a serves to illustrate the behaviour of the surface electron temperature under USP irradiation. One can see that the temperature $T_e^{\mathrm{kin}}(t)$ initially grows faster, i.e. heating is closer to the adiabatic one. Subsequently, a more intense energy outflow from the surface has the effect that the $T_e^{\mathrm{kin}}(t)$ curve runs lower than the $T_e^{\mathrm{ttm}}(t)$ curve. The relative error in the TTM calculation of the maximum electron temperature is equal to 13% in this case. It is precisely the difference $T_e^{\mathrm{ttm}}(t) - T_e^{\mathrm{kin}}(t) > 0$, which persists practically throughout

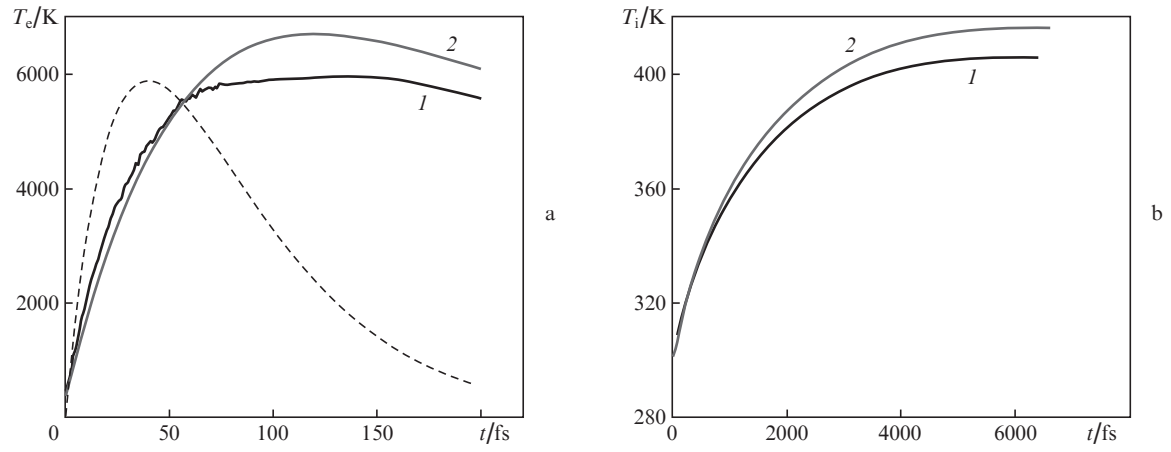

Figure 8. Time dependences of the (a) electron and (b) lattice temperatures at the surface of silver calculated in the framework of the model reliant on the kinetic equation (*1*) and the TTM (*2*) (the dashed curve shows the pulse shape).

the two-temperature stage, underlies the difference in the final (maximal) lattice temperature. The effect of the form of non-equilibrium distribution function on the electron–lattice energy exchange is negligible because the thermalisation time throughout the depth is short in comparison with the characteristic equilibration time for the electron and lattice temperatures, which is consistent with the data of Ref. [6]. The relative error of calculating the increment of lattice temperature amounts to 10% per pulse.

Supposedly the behaviour of the electron temperature may be explained as follows. The TTM proceeds from the Fourier law, which implies proportionality of the thermal flux at some point in time to the temperature gradient at the same point in time. In reality, the thermal flux induced in the medium under ultrafast heating will be somewhat retarded relative to the rapidly varying temperature gradient. Therefore, early in the pulsed irradiation, when the heating rate is high, the transfer of energy does not manage to remove it from the surface layers, which causes a somewhat faster growth rate of the electron temperature during the pulse rise. Subsequently, this effect becomes less significant, and beginning from the point in time $t \approx 40$ fs, as is clear from Fig. 6a, the energy outflow from the surface becomes more intense. The Fourier law implies that the electron free path is short in comparison with the heating gradient scale length. For $T_e \approx 5000$ K, the free path is equal to about 10 nm and is comparable to the radiation penetration depth ($\delta = 10$ nm), which determines the characteristic temperature gradient scale length. The hot electrons from the surface traverse a distance δ in a time $\delta/v \approx 10$ fs ($v \approx 10^6$ m s^{-1} is the characteristic electron velocity) and foster the enhanced energy removal from the skin layer. To this there corresponds the lowering of the heating rate in the 30–140 fs interval in Fig. 8a. Next, as the energy is removed from the skin layer, the heating gradient scale length becomes larger and the further metal cooling may be described using the TTM.

Increasing the pulse energy density leads to an increase in electron–electron collision frequency and shortens the electron free path. Consequently, the error of TTM temperature calculations lowers with an increase in pulse energy density. Figure 9 shows the relative errors of TTM-based calculations of the maximum electron [$\delta_T(T_e)$] and lattice [$\delta_T(T_i)$] temperatures for silver and aluminium as functions of absorbed energy density (the curves are plotted for $t_0 = 40$ fs). If it is assumed that the maximum admissible error level is equal to 10%, the boundary energy density $Q_T(T_e)$ above which the traditional two-temperature approach may be

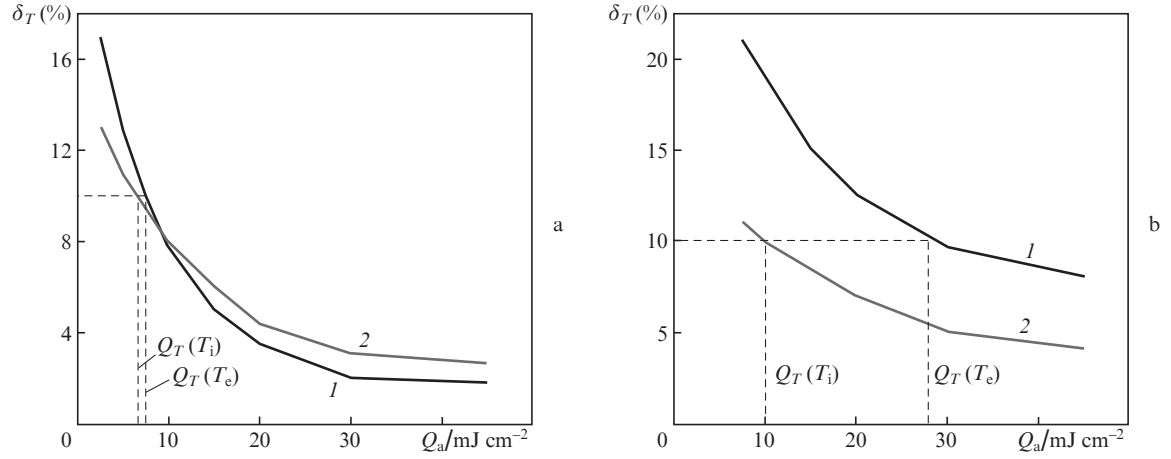

Figure 9. Errors of TTM calculations of the maximum electron (*1*) and lattice (*2*) temperatures for (a) silver and (b) aluminium.

regarded as adequate for calculating the maximal electron temperature is equal to 7.5 mJ cm^{-2} for silver and to 28 mJ cm^{-2} for aluminium. In the calculation of lattice heating, the boundary energy density $Q_T(T_i)$ amounts to 6.7 mJ cm^{-2} and 10 mJ cm^{-2} for silver and aluminium, respectively. In the case of silver, the $Q_T(T_i)$ value is appreciable lower than the melting threshold energy density, which is equal to 35 mJ cm^{-2}, according to simulations (by a melting threshold is meant the minimal absorbed energy density required for attaining the melting temperature at the surface; here we do not consider the issues related to the possible lattice heating above the melting temperature under USP irradiation of the metal). In the case of aluminium, $Q_T(T_i)$ is close to the melting threshold.

Influence of electron temperature dynamics on electron emission. Owing to a strong dependence of thermal electron emission on the surface electron temperature, even a small error in its calculation may lead to significant changes in emission current density and, as a consequence, in the total number of emission electrons. Figure 10 shows the time dependences of the emission current density, which were calculated in the framework of the TTM and the model proposed in our work, for $Q_a = 5$ mJ cm^{-2} and $t_0 = 40$ fs for silver (the dynamics of the surface electron temperature in this case is shown in Fig. 8a). We emphasise that we are dealing with only the flux of electrons emanating from the surface; in reality, a fraction of the outgoing electrons will return back. The contribution to the total number of escape electrons arising from the time interval $t < \tau_0^{em}$ is negligible. As is evident from Fig. 10, TTM calculations markedly overrate the emission current density. The total number of electrons emitted from the surface is approximately 2.5 times smaller than the TTM-predicted number for this processing mode. Plotted in Fig. 11 is the relative error of calculation of the total number of electrons emitted per unit area in relation to absorbed energy density for silver and aluminium. By estimating the limit of TTM applicability as regards emission effects at a level of 10%, we see that the TTM works for $Q_a > 30$ mJ cm^{-2} in the heating of silver and for $Q_a > 70$ mJ cm^{-2} in the heating of aluminium.

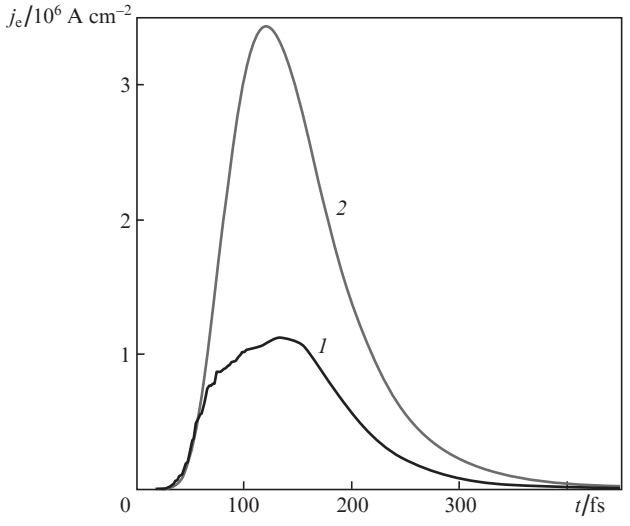

Figure 10. Time dependences of the electron emission current density calculated proceeding from the kinetic equation (*1*) and the TTM (*2*).

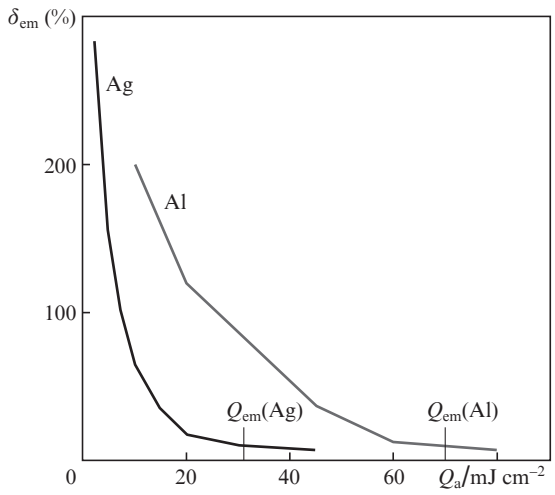

Figure 11. Relative error of TTM calculations of the total number of emission electrons for silver and aluminium for $t_0 = 40$ fs.

4. Conclusions

To summarise, we outline the main results of our work. The electron thermalisation time in the skin layers of typical metals (silver, aluminium) under irradiation by USPs which give rise to ablation ($Q_a \approx 100$ mJ cm^{-2}) does not exceed 45 fs, and so the heating by such pulses may be described in the framework of the TTM. The thermalisation time becomes longer with a decrease in pulse energy density and amounts to hundreds of femtoseconds for $Q_a \approx 2.5$ mJ cm^{-2}. The high-energy tail of the distribution function develops much faster than the equilibrium distribution function as a whole, and emission processes may be described using the notion of temperature throughout the energy density range under consideration (2.5–300 mJ cm^{-2}). An analysis of the heating with the inclusion energy transport showed that a TTM-based calculation has a certain error, which depends on the processing mode. In the calculation of the maximum electron temperature, the limits of TTM applicability in absorbed energy density amount to 7.5 mJ cm^{-2} for silver and to 28 mJ cm^{-2} for aluminium, assuming that the greatest admissible error is equal to 10%. In the calculation of the maximum lattice temperature, the limits are equal to 6.7 mJ cm^{-2} for silver and to 10 mJ cm^{-2} for aluminium. The departures seen in the dynamics of the surface electron temperature are responsible for an appreciable lowering of the emission current and the total number of emitted electrons. In the calculation of the total number of electrons emitted per unit surface, the limits of TTM applicability in absorbed energy density amount to 30 mJ cm^{-2} for silver and to 70 mJ cm^{-2} for aluminium for a 10% error.

The boundary values for pulse energy density determined in our work allow the following conclusions. In the analysis of the lattice heating of bulk metals (silver, aluminium) by an USP with an energy density above the melting threshold, use can be made of the traditional TTM, while the kinetic approach is preferred for an energy deposition below the melting threshold. In the analysis of electron emission from the surface of a bulk metal irradiated by an USP, the TTM may be applied for an energy input above the ablation threshold for aluminium and above the melting threshold for silver.

Acknowledgements. This work was supported by the Russian Science Foundation (Agreement No. 14-12-00351).

References

1. Anisimov S.I., Imas Ya.A., Romanov G.S., Khodyko Yu.V. *Deistvie izlucheniya bol'shoi moshchnosti na metally* (Effect of High-Power Radiation on Metals) (Moscow: Nauka, 1970).
2. Fann W.S., Storz R., Tom H.W.K. *Phys. Rev. B*, **46**, 13592 (1992).
3. Faure J. et al. *Phys. Rev. B*, **88**, 075120 (2013).
4. Merschdorf M., Kennerknecht C., Willig K., Pfeiffer W. *New J. Phys.*, **4**, 95 (2002).
5. Mueller B.Y., Rethfeld B. *Phys. Rev. B*, **87**, 035139 (2013).
6. Rethfeld B., Kaiser A., Vicanek M., Simon G. *Phys. Rev. B*, **65**, 214303 (2002).
7. Gamaly E.G. *Phys. Rep.*, **508**, 91 (2011).
8. Veiko V.P., Jarchuk M.V., Ivanov A.V. *Laser Phys.*, **22**, 1310 (2012).
9. Yakovlev E.B., Sergaeva O.N., Svirina V.V., Yarchuk M.V. *Proc. SPIE Int. Soc. Opt. Eng.*, **9065**, 906509 (2013).
10. Hufner S. *Photoelectron Spectroscopy: Principles and Applications* (Berlin: Springer-Verlag, 1995).
11. Petrov Yu.V., Inogamov N.A., Migdal K.P. *Pis'ma Zh. Eksp. Teor. Fiz*., **97**, 24 (2013) [*JETP Lett*., **97**, 20 (2013)].
12. Bulgakova N.M., Stoian R., Rozenfeld A. *Kvantovaya Elektron.*, **40**, 966 (2010) [*Quantum Electron*., **40**, 966 (2010)].
13. Dyukin R.V., Martsinovskiy G.A., Sergaeva O.N., Shandybina G.D., Svirina V.V., Yakovlev E.B. In: *Laser Pulses – Theory, Technology and Applications*. Ed. by I. Peshko (Rijeka: InTech, 2012) Ch. 7.
14. Gurov K.P. *Osnovaniya kineticheskoi teorii* (Foundations of Kinetic Theory) (Moscow: Nauka, 1966).
15. Ashcroft N.W., Mermin N.D. *Solid State Physics* (New York: Holt, Rinehart and Winston, 1976; Moscow: Mir, 1979).
16. Landau L.D., Lifshits E.M. *Quantum Mechanics: Non-Relativistic Theory* (Oxford: Pergamon Press, 1977; Moscow: Nauka, 1989).
17. Bass F.G., Gurevich Yu.G. *Goryachie elektrony i sil'nye elektromagnitnye volny v plazme poluprovodnikov i gazovogo razryada* (Hot Electrons and Strong Electromagnetic Waves in Semiconductor and Gas Discharge Plasmas) (Moscow: Nauka, 1984).
18. Veiko V.P., Libenson M.N., Chervyakov G.G., Yakovlev E.B. *Vzaimodeistvie lazernogo izlucheniya s veshchestvom. Silovaya optika* (Interaction of Laser Radiation with Substance. Power Optics) (Moscow: Fizmatlit, 2008).
19. Belotserkovskii O.M. *Chislennoe modelirovanie v mekhanike sploshnykh sred* (Numerical Simulation in Mechanics of Continuous Media) (Moscow: Nauka, 1984).
20. Gasparov V.A., Huguenin R. *Adv. Phys*., **42**, 393 (1993).
21. Inogamov N.A., Petrov Yu.V. *Zh. Eksp. Teor. Fiz*., **137**, 505 (2010) [*JETP*, **110**, 446 (2010)].